coatings

MDPI

Article

Obtaining of Antibacterial Nanoporous Layer on Ti7.5Mo Alloy Surface Combining Alkaline Treatment and Silver: In Vitro Studies

Barbara Lois Mathias de Souza [1], Ana Lúcia do Amaral Escada [2], Célio Junior da Costa Fernandes [3], Gerson Santos de Almeida [3], Willian Fernando Zambuzzi [3], Patricia Capellato [4], Daniela Sachs [4] and Ana Paula Rosifini Alves [1,2,*]

1 Unesp, São Paulo State Univesity, School of Engineering and Sciences, Guaratinguetá Campus, São Paulo 12516-000, SP, Brazil; barbara.lois@unesp.br
2 Unesp, São Paulo State University, School of Engineering, Ilha Solteira Campus, São Paulo 15385-000, SP, Brazil; ala.escada@unesp.br
3 Unesp, São Paulo State University, Institute of Biosciences, Distrito de Rubião Júnior, s/n, Rubião Junior 18618-970, SP, Brazil; celio.jf15@gmail.com (C.J.d.C.F.); gs.almeida@unesp.br (G.S.d.A.); w.zambuzzi@unesp.br (W.F.Z.)
4 Unifei—Federal University of Itajubá, Institute of Physics and Chemistry, Itajubá 37500-903, MG, Brazil; pat_capellato@yahoo.com.br (P.C.)
* Correspondence: paula.rosifini@unesp.br

Abstract: In the present study, a combination of alkaline treatment and silver was used to produce an antibacterial nanolayer on the Ti7.5Mo alloy surface. The antibacterial response and osteogenesis were evaluated by assessing the adhesion and proliferation of *S. aureus* and *S. epidermidis*, as well as the adhesion, viability, and expression levels of genes involved in osteogenic differentiation in the mouse pre-osteoblast cell line MC3T3-E1. The potential stimulus of extracellular remodeling was evaluated using zymography. Our results showed that there is no difference in cytotoxicity after silver immobilization. Protein activity (MMP9) progressively increased for theTi7.5Mo alloy, both untreated and after alkaline treatment. However, the highest increase in protein activity was observed when the alloy was in direct contact with immobilized silver nanoparticles. The surfaces containing silver showed a better response in terms of colony formation, meaning that less bacterial adhesion was detected. The results showed that the layer formed was effective in reducing bacterial activity without altering cell viability.

Keywords: silver; biocompatibility; chemical method; nanoporous layer

check for updates

Citation: Mathias de Souza, B.L.; Escada, A.L.d.A.; Costa Fernandes, C.J.d.; de Almeida, G.S.; Zambuzzi, W.F.; Capellato, P.; Sachs, D.; Rosifini Alves, A.P. Obtaining of Antibacterial Nanoporous Layer on Ti7.5Mo Alloy Surface Combining Alkaline Treatment and Silver: In Vitro Studies. *Coatings* **2024**, *14*, 52. https://doi.org/10.3390/coatings14010052

Academic Editor: Ioana Demetrescu

Received: 11 October 2023
Revised: 7 December 2023
Accepted: 21 December 2023
Published: 29 December 2023

1. Introduction

Metal implants have been used in the manufacturing of devices to replace hard tissues such as orthopedic, dental, and cardiovascular implants. Titanium and its alloys play an important role due to their bulk properties, such as high mechanical resistance, low elastic modulus, and fatigue strength, which are associated with their excellent biocompatibility [1–4]. The Ti–7.5Mo (%wt) alloy has been developed by Lin et al. [5] and possesses an α'' phase structure as well as a low modulus of 65 GPa; therefore, it is recommended for applications such as biomedical implants.

Despite its excellent properties, these materials are foreign bodies that may affect the immune system, creating a site susceptible to bacterial attack, including opportunistic bacteria with weak virulence. Infections can occur in a short time (within 1 month), while late infections develop after more than 1 month, which are difficult to diagnose accurately. *S. aureus* is often associated with acute implant infections, while *S. epidermidis* often causes late chronic infections. This local infection is one of the biggest factors associated with implant failure which can be characterized by pain, swelling, and loss of function [6].

Nowadays, the treatment of these infections involves administering high doses of systemic antibiotics for extended periods of time. However, this approach can lead to numerous side effects and is often ineffective in achieving a cure. Therefore, several studies have been conducted related to the development of antimicrobial surfaces [7].

Surface modification techniques associated with the immobilization of bactericidal metallic agents can serve as an alternative for functionalizing these materials. Several methods have been developed, including chemical methods such as alkaline treatment [8–10], anodic oxidation [11–13], chemical vapor deposition [14,15], and sol-gel [16,17]. Alkaline treatment is a surface modification method that utilizes an NaOH solution at various concentrations and has been extensively studied.

Another method used is the mobilization of bactericidal agents associated with surface treatment. The mechanism of the antibacterial action of silver can occur through the release of silver ions or through direct contact of silver with bacteria. Its antimicrobial properties are achieved by using silver salts, such as silver nitrate ($AgNO_3$), on a nanometric scale that decompose to release silver ions (Ag+). The electrostatic interaction between the positive charge of silver and the negative charge of the bacterial membrane increases the permeability of the membrane, allowing for the diffusion of Ag+ ions into the cells [18]. Silver nanoparticles (AgNPs) can easily penetrate the microbial cell wall due to their small size [19]. The silver nanoform is more reactive and can cross cell membranes, leading to the deposition of intracellular nanoparticles that cause cell dysfunction [18].

In previous studies conducted by our group [11,12,20,21], we utilized two different types of surface treatment techniques, namely alkaline treatment and anodic oxidation, on the Ti7.5Mo alloy. The anodic oxidation process occurs in an electrochemical cell, consisting of two electrodes: a titanium anode and a platinum cathode. When a constant current or voltage is applied between the anode and the cathode, the oxidation and reduction reactions, in combination with the diffusion of ions in the electrolyte, lead to the formation of a porous TiO_2 layer on the surface of the anode [11,12]. In alkaline treatment with sodium hydroxide, the TiO_2 layer dissolves in the alkaline solution because of attacks by hydroxyl groups. This reaction occurs simultaneously with the hydration of titanium. An attack on the hydroxyl of the further hydrated TiO_2 produces negatively charged hydrates that incorporate Na+ ions and produce a porous layer of bioactive sodium titanate hydrogel [21]. Both methods result in an improved cell response. In addition, the incorporation of silver into the surface of the Ti7.5Mo alloy with TiO_2 nanotubes, using polydopamine as a linker, resulted in the inhibition of *S. aureus* growth [12].

Thus, to advance the group's research on surface modification of titanium alloys, the objective of this study was to produce a nanoporous layer combining alkaline treatment and silver. The chemical methods are particularly easy to perform, are of low cost, and could be an alternative route for producing bactericidal surfaces on titanium-based alloys.

2. Materials and Methods

2.1. Processing of the Ti7.5Mo Alloy

The Ti–7.5Mo (%wt) alloy was produced from sheets of commercially pure titanium and molybdenum. Samples were melted in an arc furnace with an argon atmosphere. The ingots were homogenized under vacuum at 1100 °C for 24 h and then cold-worked by swaging, resulting in bars with a diameter of 10 mm.

2.2. Surface Treatment

For the surface treatment, discs with 3 mm of thickness were cut from bars and ground with SiC sandpaper (#100), cleaned in an ultrasonic bath with isopropyl alcohol for 5 min, washed individually with deionized water, and then were subjected to alkaline treatment. The protocol developed in previous studies by our group for alkaline treatment [21–23] was modified to include silver immobilization in the treatment. Samples were immersed in a 5 M solution of sodium hydroxide (NaOH) at 80 °C for 72 h and then washed with deionized water and dried at 60 °C for 24 h. Following this, the samples were immersed in

a solution prepared with 2.15 g of $AgNO_3$ (Sigma Aldrich, St. Louis, MO, USA) and 250 mL of deionized water at 60 °C for 18 h. Afterward, they were annealed in an electric furnace at 450 °C for 1 h. The samples were divided into three groups for analysis based on the type of surface treatment: ground surface (the control group G1), alkaline treatment (G2), and alkaline treatment with silver immobilization (G3).

2.3. Surface Characterization

A scanning electron microscope (SEM, LEO 1450 VP, Zeiss, Oberkochen, Germany) was used to analyze the surface morphology and elemental concentration of the Ti7.5Mo alloy surface using EDS analysis. The surface topography of the substrate was characterized using an optical profilometer (Weeco NT 1100, São José dos Campos, Brasil). Contact angles were obtained using the sessile drop method with Krüss equipment. The initial volume of distilled water was 5 µL, and the measurements were performed at room temperature.

2.4. Biocompatibility Study

Figure 1 shows a schematic representation of the techniques used to assess the biocompatibility of the surface treatments studied.

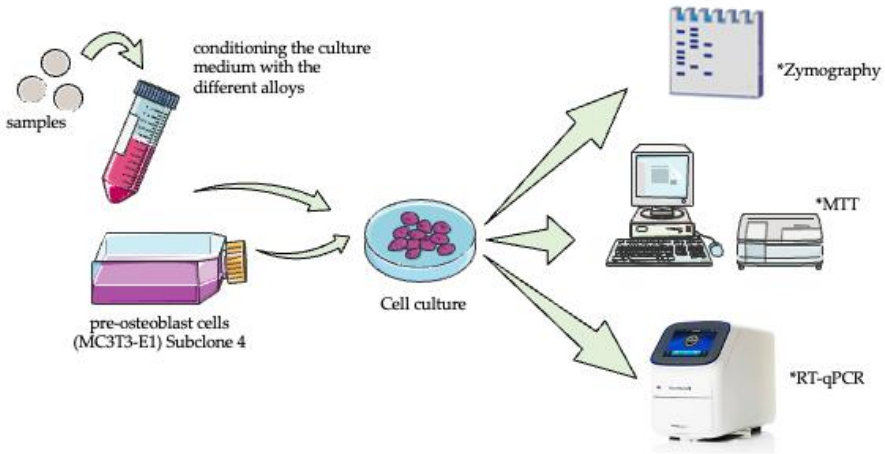

Figure 1. Schematic representation of the techniques used to evaluate the biocompatibility of the surface treatments.

2.4.1. Cell Viability and Adhesion Assays

Pre-osteoblasts (MC3T3-E1 subclone 4) were cultured in an Alpha-MEM medium supplemented with 10% fetal bovine serum (FBS) and antibiotics (100 U/mL penicillin and streptomycin 100 mg/mL) and kept in an oven at 37 °C and 5% CO_2.

To verify the cytotoxic potential, the alloys were kept in a culture medium for 24 h. After the period of conditioning, the medium was collected and supplemented with 10% fetal bovine serum (FBS) and used to treat pre-osteoblasts of the lineage MC3T3-E1 subclone 4 for a period of 24 h. The cells were plated 24 h before treatment in a 96-well plate and at the density of 5×10^4 cells/mL. After the specified time of exposure to the conditioned medium, the viability of these cells was measured by the MTT test. Where the culture medium was removed, Thiazolyl Blue Tetrazolium Bromide salt 1 mg/mL was added and placed in an oven for an additional 3 h. After this period, the medium was removed, and 0.1 mL of DMSO for the solubilization of the dye was formed by viable cells. Afterward, the absorbance was measured at 570 nm using a microplate reader.

Pre-osteoblasts were plated with a medium conditioned by the alloys. The cells were seeded in 96-well plates at a density of 5×10^4 cells/mL. After 24 h of treatment, the medium was removed, and adhesion was measured by the incorporation of Crystal Violet. The absorbance was measured at 540 nm on a microplate reader.

2.4.2. Gene Expression by RT-qPCR

The total RNA was extracted utilizing the TRIzol/chloroform protocol. Subsequently, the concentration and purity of the extracted RNA were assessed employing a microplate reader (SYNERGY-HTX multi-mode reader, Biotek, Tigan St, Winooski, VT, USA). For gene expression analysis, initial cDNA synthesis was conducted using the High-Capacity cDNA Reverse Transcription Kit (Applied Biosystems, Foster City, CA, USA) following the manufacturer's instructions post DNase I treatment (Invitrogen, Carlsbad, CA, USA). Subsequently, quantitative PCR (qPCR) reactions were executed in a QuantStudio®3 Real-Time PCR instrument (Thermo Fisher Scientific, Waltham, MA, USA) with 10 µL reaction volumes (Syber Green Master Mix 2x (5 µL), 0.4 µmolL^{-1} of each primer [refer to Table 1 for primers and conditions], 50 ng of cDNA, and nuclease-free H_2O). The Gapdh gene served as the housekeeping gene.

Table 1. Primer sequences and details of the cycle conditions.

Gene	Primer	5′-3′ Sequence	Parameters
Integrin α1	Forward Reverse	TATCCTCCTGAGCGCCTTT TGGCCTTTTGAAGAATCCAA	95 °C-15 s; 60 °C-30 s; 72 °C-60 s
Integrin β1	Forward Reverse	CTGATTGGCTGGAGGAATGT TGAGCAATTGAAGGATAATCATAG	95 °C-15 s; 60 °C-30 s; 72 °C-60 s
Src	Forward Reverse	TCGTGAGGGAGAGTGAGAC GCGGGAGGTGATGTAGAAAC	95 °C-15 s; 60 °C-30 s; 72 °C-60 s
FAK	Forward Reverse	TCCACCAAAGAAACCACCTC ACGGCTTGACACCCTCATT	95 °C-15 s; 60 °C-30 s; 72 °C-60 s
Cofilin	Forward Reverse	CAGACAAGGACTGCCGCTAT TTGCTCTTGAGGGGTGCATT	95 °C-15 s; 60 °C-30 s; 72 °C-60 s
GAPDH	Forward Reverse	AGGCCGGTGCTGAGTATGTC TGCCTGCTTCACCACCTTCT	95 °C-15 s; 60 °C-30 s; 72 °C-60 s
Runx2	Forward Reverse	GGACGAGGCAAGAGTTTCA TGGTGCAGAGTTCAGGGAG	95 °C-15 s; 60 °C-30 s; 72 °C-60 s
Osterix	Forward Reverse	CCCTTCCCTCACTCATTTCC CAACCGCCTTGGGCTTAT	95 °C-15 s; 60 °C-30 s; 72 °C-60 s
Osteocalcin	Forward Reverse	AGACTCCGGCGCTACCTT CTCGTCACAAGCAGGGTTAAG	95 °C-15 s; 60 °C-30 s; 72 °C-60 s
MMP2	Forward Reverse	AACTTTGAGAAGGATGGCAAGT TGCCACCCATGGTAAACAA	95 °C-15 s; 60 °C-30 s; 72 °C-60 s
MMP9	Forward Reverse	TGTGCCCTGGAACTCACACGAC ACGTCGTCCACCTGGTTCACCT	95 °C-15 s; 60 °C-30 s; 72 °C-60 s

2.4.3. Zymography

The conditioned medium was harvested after 7 days to estimate the stimulus of extracellular matrix remodeling by measuring the activities of MMPs through the zymography assay. The culture medium obtained with osteoblasts was centrifuged at 14,000 rpm for 15 min to avoid cell debris and, later, the protein concentration was determined by the Lowry method. The same amount of protein was dissolved in gel (12% polyacrylamide and 4% gelatin). Subsequently, renaturation in aqueous Triton X-100 solution (2% *w*/*v*), was incubated for 18 h in a proteolysis buffer at 37 °C and stained with 0.05% dye solution for 3 h. The gels were washed in 30% methanol solution (*v*/*v*) and 10% glacial acetic acid solution (*v*/*v*). The opposite staining was obtained in the gels where the gelatinolytic activity (bands) of matrix metalloproteinases 2 (MMP2, ~62 kDa) and 9 (MMP9, ~84 kDa) were then analyzed using ImageJ software, open-source image processing platform (http://imagej.net).

2.5. Bacterial Cell Viability

The analysis of bacterial proliferation was performed using the reference strains *S. aureus* and *S. epidermidis*, which were seeded in brain heart agar infusion and incubated at 37 °C for 24 h. Then, the microorganism colonies were suspended in a sterile saline solution [sodium chloride (NaCl) 0.9%] and adjusted to a turbidity of 0.5 on the MacFarland scale (1.5 × 10^8 CFU/mL). Samples were plated in 24-well plates with 2 mL of BHI broth

supplemented with 5% sucrose and inoculated with 0.1 mL of the bacterial suspension. The samples were incubated at 37 °C for 48 h, and the media were changed after 24 h.

The samples were washed aseptically, placed in tubes with 10 mL of sterile saline, and then sonicated for 30 s to disperse the biofilms. The suspension was considered with a dilution factor of 10^{-1} and diluted with the addition of sterile saline to 10^{-8}. Aliquots of 0.1 mL were seeded on BHI agar plates and incubated for 24 h at 37 °C. The number of colonies was counted by Counter Num.Bat.5 Alg Starter, calculated in CFU/mL, and then transformed in log10.

The *S. aureus* and *S. epidermidis* surface adhesion of each group was evaluated using scanning electron microscopy analysis after 24 h of incubation.

Statistical analyses were performed using GraphPad Prism 7 software (GraphPad Software, Boston, MA, USA), by variance analysis (one-way ANOVA), and with Tukey's correction posttest or non-parametric analysis. The p value < 0.05 was considered statistically significant.

3. Results

3.1. Surface Characterization

The top view of the surface morphologies visualized by SEM—ground (the control group—G1), alkaline treatment (G2), and alkaline treatment with silver immobilization (G3)—can be seen in Figure 2a–c, respectively. It is possible to verify that the alkaline treatment formed a porous surface, modifying the initial surface that contained grinding marks (Figure 2b). In addition, the immersion in $AgNO_3$ did not alter the surface obtained with the alkaline treatment, as can be seen in Figure 2c.

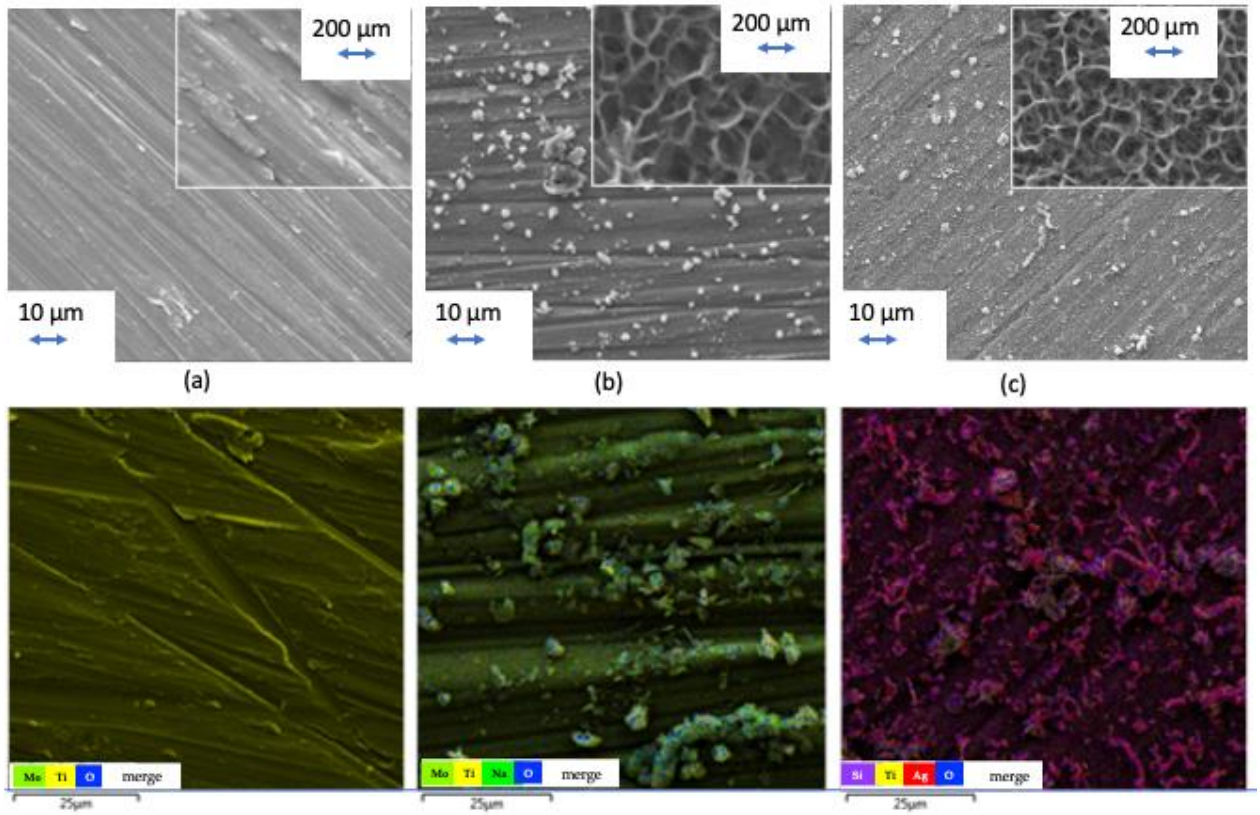

Figure 2. Morphological and chemical analyses of the Ti7.5Mo alloy after surface treatment. SEM micrograph of a top view and EDS mapping merged image: (**a**) control group (G1), (**b**) after alkaline treatment (G2), and (**c**) after alkaline treatment with silver immobilization (G3). Detail shows surface in high magnification.

EDS mapping analysis of samples from G3 (Figure 2) using EDS confirmed the presence of silver on the surface and the effectiveness of the treatment.

This difference in the topography of the Ti7.5Mo alloy after surface treatment was confirmed in 3D surface profiles and is shown in Figure 3. The average surface roughness (Ra) values were 0.48 for the control group (G1), 1.01 µm for the group with alkaline treatment (G2), and 1.52 µm for the group with alkaline treatment with silver immobilization (G3). The change in roughness led to a change in surface wettability: for the control group (G1), the angle found was 73.5° ± 0.4°. After alkaline treatment (G2), the value decreased to 1.4° ± 0.1°; after alkaline treatment with silver immobilization (G3), the measurement was 3.2° ± 0.4°. The decrease in the contact angle suggests that both treated samples increase wettability in relation to the untreated sample, characterizing a hydrophilic surface.

3.2. Biocompatibility Studies

After conditioning the culture medium with the different alloys, the medium was used to treat pre-osteoblast cells for 24 h and evaluate cytotoxicity, in addition to evaluating different messenger RNAs involved in cell adhesion and investigating the activity of MMPs by zymography.

Initially, our data show that the different alloys do not exhibit toxicity to the cells since no difference was observed between the groups treated with the control (Figure 4a). In addition, the adhesion assay, another important mechanism to investigate the death process through the incorporation of Crystal Violet vital dye, showed no difference between treatment and control (Figure 4b). Together, these initial data allowed us to investigate whether signaling pathways are being modulated, by investigating the expression of genes specifically involved with the adhesion pathway. This process occurs through the recruitment of Integrins that were shown to have increased in the osteogenic medium (OM) positive control groups. In this case, Integrin a1 and B1 were up-modulated in the OM, but only B1 was increased in the conditioned medium-treated groups when compared with the control groups (Figure 4c,d). Furthermore, we investigated the expression profile of FAK and Src, adhesion pathway proteins that were up-regulated in the G1 group compared with the other experimental groups (Figure 4e,f). Adhesion mechanisms can result in rearrangement of the cellular cytoskeleton, and this mechanism can be regulated by Cofilin. In our data, Cofilin expression showed a significant increase in the OM and G1 groups (Figure 4g). Furthermore, two important genes involved with the progress of osteoblast differentiation were evaluated. We observed that Runx2 was not modulated between the experimental groups, but Osteocalcin decreased in all groups when compared with the control group (Figure 4h,i).

In the context of the cellular microenvironment, cytoskeletal adhesion and remodeling mechanisms can be regulated by extracellular matrix remodeling, which is regulated by the activity of metalloproteinases. Our data show that the OM group had an increase in the expression of MMP2 and MMP9, while the G1–G3 groups showed a reduction in the expression of these genes (Figure 5a,b). The MMP activity was measured by zymography, and our data show that MMP9 had its activity progressively increased in the G1 < G2 < G3 groups in relation to the OM and control groups (Figure 5c–e).

3.3. Bacterial Cell Viability

In vitro studies were carried out to study the bactericidal effect of adding silver to the alkaline treatment on the surface of the Ti7.5Mo alloy, against *S. aureus* and *S. epidermidis*. The adhesion of *S. aureus* and *S. epidermidis* to the surface of each group was evaluated using scanning electron microscopy analysis after 24 h of incubation (Figure 6).

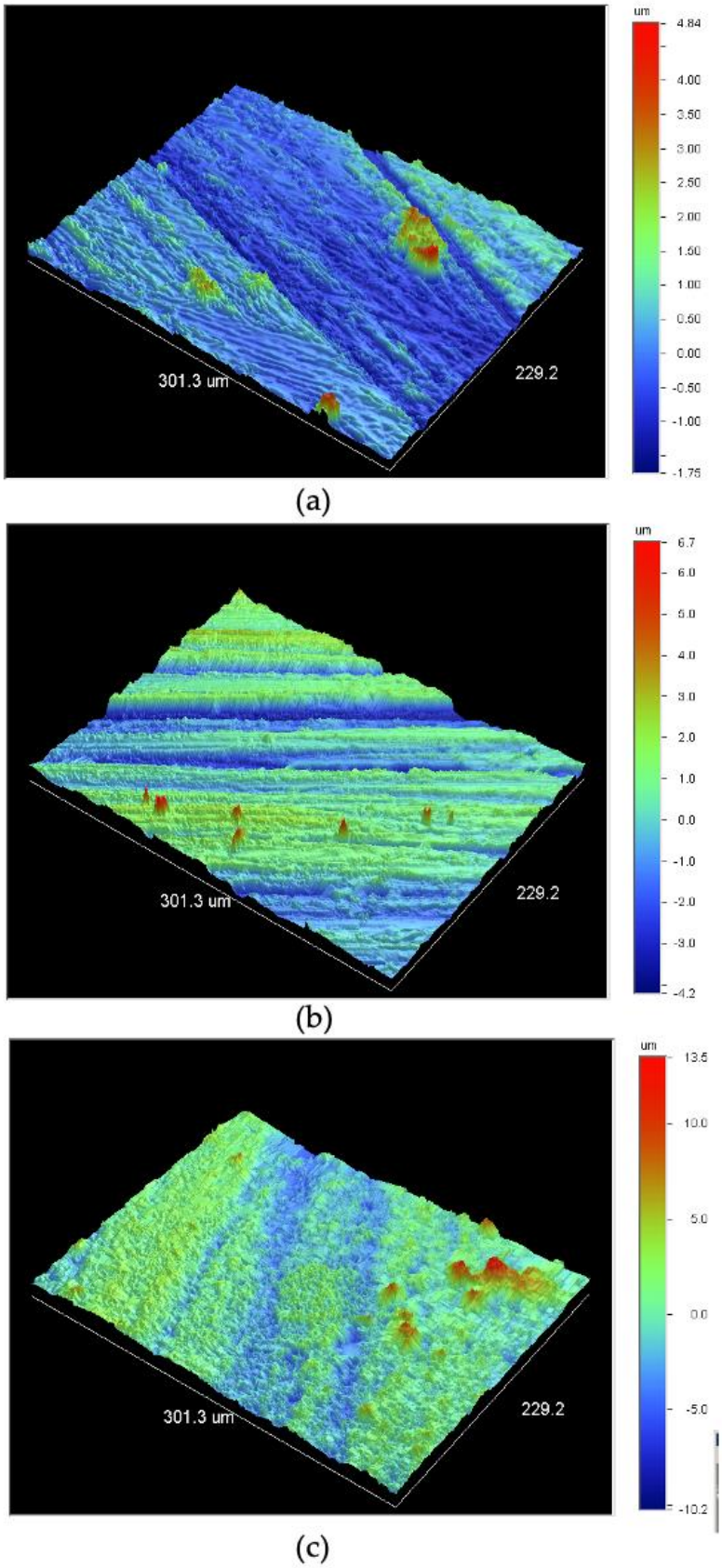

Figure 3. Topography of the Ti7.5Mo alloy after surface treatment obtained by 3D profilometry: (**a**) control group (G1), (**b**) after alkaline treatment (G2), and (**c**) after alkaline treatment with silver immobilization (G3).

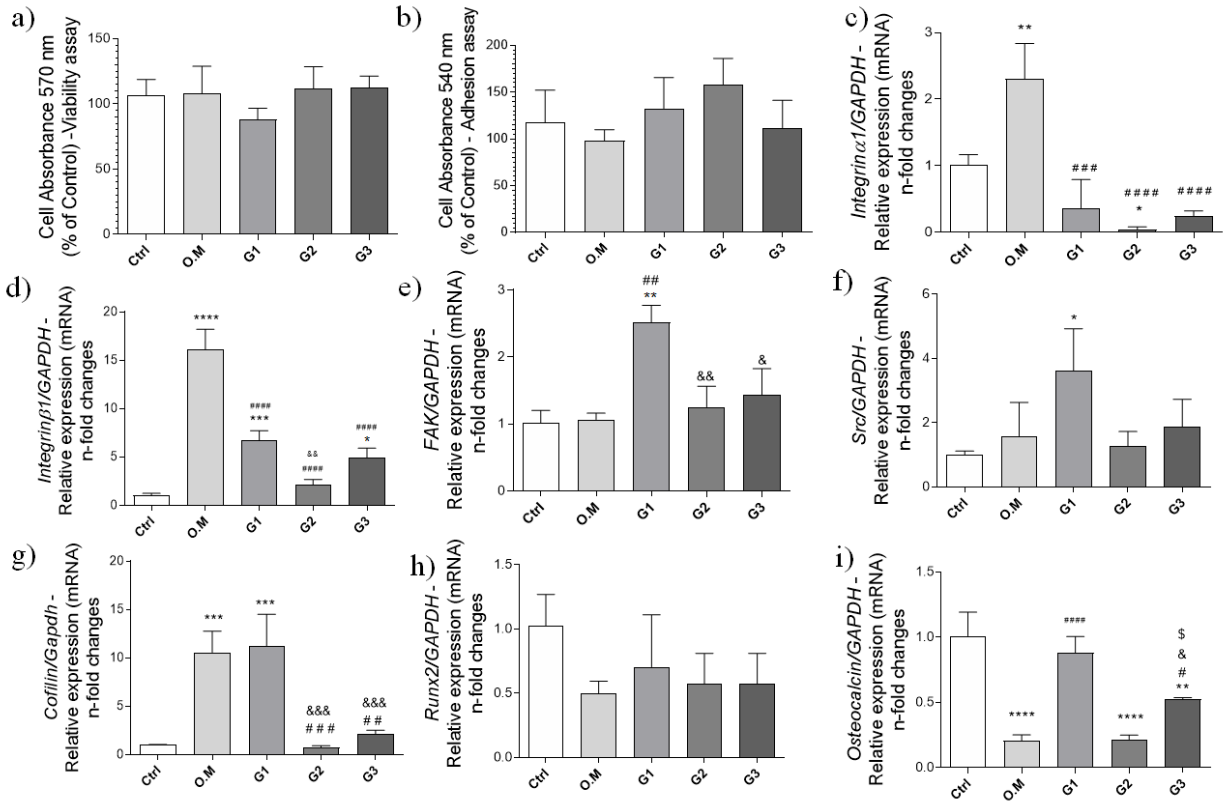

Figure 4. Biological and cytotoxicity assays. (**a**) MTT cell viability assay; for each group n = 6. (**b**) Crystal Violet adhesion assay; for each group n = 6. Gene expression groups—(**c**) Integrin α1; (**d**) Integrin β1; (**e**) FAK; (**f**) Src; (**g**) Cofilin; (**h**) Runx2; and (**i**) Osteocalcin. All gene expression groups were n = 3.

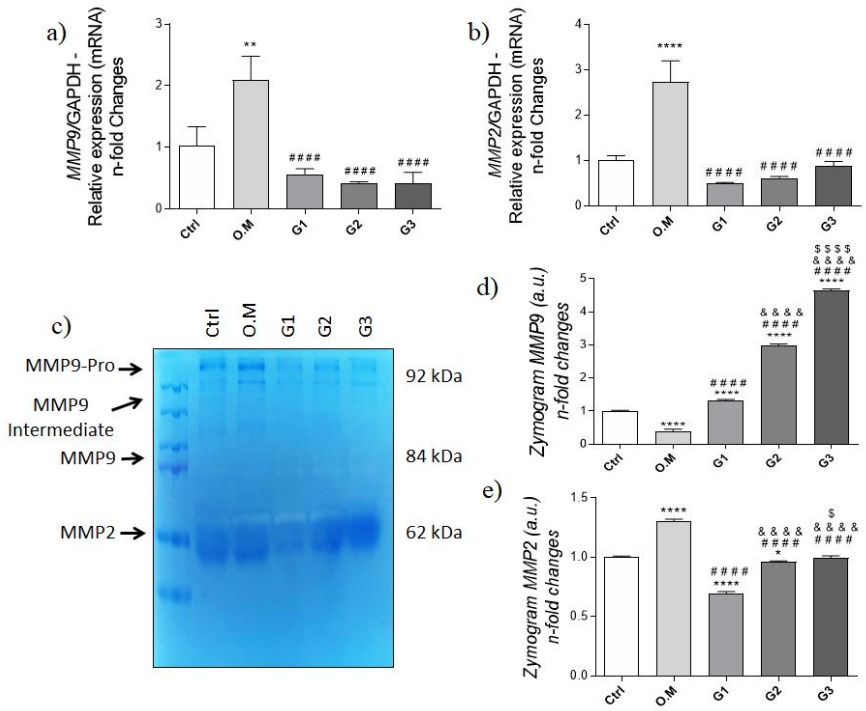

Figure 5. MMP expression and zymography activity: (**a**) expression of MMP9 gene; (**b**) MMP2 gene expression; (**c**) zymography gel; (**d**) quantification of MMP9 band; and (**e**) quantification of MMP2 bands.

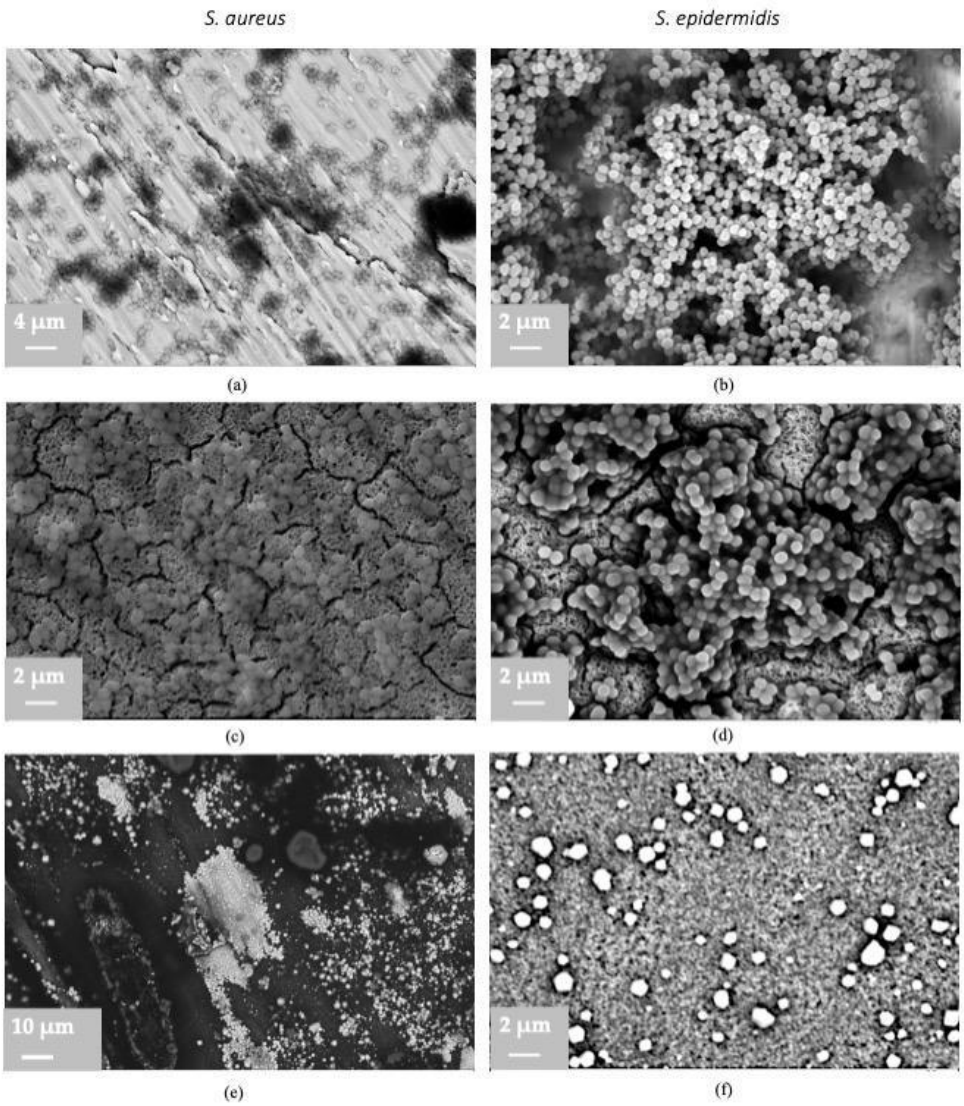

Figure 6. Comparative micrographs of the surfaces for *S. aureus*: (**a**) Ti7.5Mo alloy (G1), (**c**) Ti7.5Mo alloy after alkaline treatment (G2), and (**e**) after alkaline treatment and silver immobilization (G3); and for *S. Epidermidis*: (**b**) Ti7.5Mo alloy (G1), (**d**) alkaline treatments (G2), and (**f**) alkaline treatment and silver immobilization (G3).

According to the micrographs, it is possible to observe for samples from group G1 and G2 the *S. aureus* biofilm formation over the surface, containing some voids (Figure 6a,b). On the other hand, for samples containing silver, there was less adhesion of bacteria with the formation of small scattered colonies (Figure 6c).

In relation to the *S. epidermidis* adhesion, the formation of bacteria clusters occurred for groups G1 and G2, which were not found in samples containing silver (Figure 6d,e). In this case, the presence of isolated bacterial cells was observed along the surface (Figure 6f). The behavior shown for both bacteria types confirmed the bactericidal effect of silver.

In the histogram (Figure 7), the values of CFU (Colony Forming Units) for the bacteria *S. aureus* do not show significant differences comparing G1 with G2 but do show less colony formation for G3. In relation to *S. epidermidis*, samples G2 and G3 showed less colony formation compared with *S. aureus*.

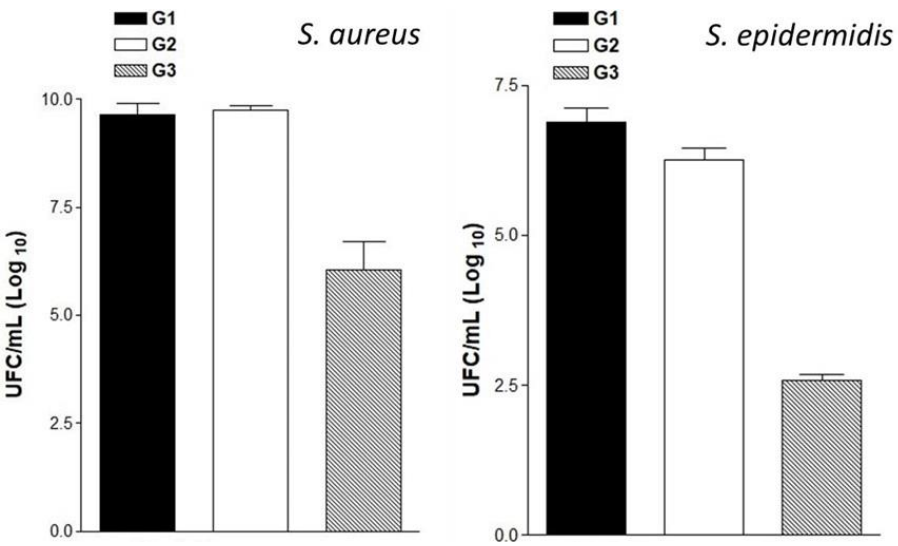

Figure 7. Comparative histogram of CFU (Colony Forming Units) for *S. aureus* and *S. epidermidis* bacteria obtained through Student's *t* test ($p < 0.05$).

4. Discussion

The bioactivity on the surface of the material is a very important property that is able to improve the response between the bone and the implant. According to Kim et al. (2021), by optimizing the surface chemistry of biomaterials, the events that begin with the initial protein and cell adhesion, the immune response and cell behavior can be controlled [24]. In this study, alkaline treatment to induce bioactivity on the surface of the Ti7.5Mo alloy was realized. In Figure 2, it is possible to observe the image obtained in the electron microscope scan for the control sample (Figure 2a), where the TiO_2 passive layer that formed has grooves and a flat surface. After immersion in 5M NaOH for 72 h at 80 °C, the passive O–metal layer dissolves to form OH–metal, and a homogeneous porous film of sodium titanate forms (Figure 2b). The formation of the sodium titanate layer is a condition that has already been well studied [19,20], and it was confirmed by EDS, with the presence of the element sodium (Na), as shown in Figure 2b. Furthermore, immersion in $AgNO_3$ (diluid in deionized water) did not change the morphology of the surface obtained with the alkaline treatment, likely because the solution was absorbed by the porous layer, as can be seen in the EDS mapping merged image (Figure 2c). The presence of silver in the top layer offers a biocidal advantage. Silver has long been known to be one of the most promising antibacterial agents. Any dissolved silver released from the coating will be directly toxic to microorganisms [25,26].

Many studies have already demonstrated that surface topographic promotion of osseointegration depends on the ability to induce differentiation of pluripotent mesenchymal stem cells to the osteoblastic lineage and stimulate matrix secretion by osteoblasts [27–30]. The surface of a material can induce/promote cell differentiation from the contact of the cells with the surface. Depending on whether the surface is favorable for adhesion, a signaling cascade of molecules, proteins, and factors that modulate the responses will begin, and proliferation and differentiation for osseointegration or even fibrosis of the adjacent tissue may occur. It has been shown that rough surfaces considerably improve the bond strength between implants and bone tissue and increase the rate of bone regeneration as well [31,32]. By increasing surface roughness, an increase in the rate of osseointegration and biomechanical fixation of titanium implants was observed [33]. The 3D surface profiles and the results of average surface roughness measurements of all the Ti7.5Mo alloy disks are shown in Figure 3. The average surface roughness values (Ra) of the groups studied were 0.48 µm for the control group (G1), 1.01 µm for the group with alkaline treatment (G2), and 1.52 µm for the group with alkaline treatment and silver coating (G3). Before the alkaline treatment, the control disc sample (G1) presented a less rough surface when

compared with untreated discs. After the alkaline treatment (G2) and silver coating (G3), the highest roughness was found for the group coated with silver; therefore, the addition of silver increased the roughness. According to the literature, very smooth surfaces do not allow cell fixation, and roughness values between 1 and 2 μm are preferred by osteoblasts [34]. The roughness values obtained here are consistent and in agreement with previous studies as well [26,35]. Furthermore, according to Barthes et al. (2020) [36], for contact with bone tissue, treatments that induce microscale roughness (0.2–2 μm) are widely used and clinically proven to improve osseointegration. Microtopographies with size ranges of the same magnitude as the cellular dimensions promote the formation of focal points of osteoblast adhesion and bone deposition. To obtain a good compromise between osteoblastic adhesion/proliferation and bone–implant entanglement—avoiding increased ion release, proinflammatory response, and introduction of any element that weakens the implant structure (less resistance to fatigue)—the size of the roughness should be around 0.2–2 μm [26].

Another important surface property of biomaterials is wettability, and it is related to the differences observed during cell proliferation in culture, which can affect their biocompatibility. Factors such as roughness, topography, and surface composition play an important role in a favorable result. All these features could be connected since surface structure and roughness are key parameters for the wettability profile, which will change the way bone cells proliferate on the surface. It has also been found that nanometer-sized topographies can be useful to reduce bacterial adhesion [37].

The contact angle refers to the angle that the liquid surface forms when it encounters a solid, and its measurement is the most common method to assess wettability. The value mainly depends on the relationship between the adhesive forces between the liquid with the solid and the cohesive forces of the liquid [38]. For the control group (G1), the angle found was $73.5° \pm 0.4°$. After alkaline treatment, the value decreased to $1.4° \pm 0.1°$; after silver immobilization, the measurement was $3.2° \pm 0.4°$. The decrease in the contact angle suggests that both treated samples increase wettability in relation to the untreated sample, characterizing a hydrophilic surface, which was formed due to the presence of cavernous pores by the action of NaOH, proving that chemical modifications result in a surface with high wettability and high surface energy [39]. It is also observed that hydrophilicity was inversely proportional to the increase in roughness; that is, the greater the contact angle, the lower the mean roughness Ra.

Due to the low contact angle obtained for samples with alkaline treatment (G2) and immobilized silver (G3), we can consider these surfaces ultra-hydrophilic, with a greater affinity for proteins, an ability to maintain the proper conformation and function of absorbed proteins and, subsequently, an ability to stimulate the adhesion and migration of cells. In addition, these surfaces have the ability to promote the differentiation and maturation of osteoblasts [40]. Another important factor related to the ultra-hydrophilic surface obtained in the samples with immobilized silver (G3) is that the preference for hydrophilic/hydrophobic surfaces differs between bacterial species [41]. Some studies have already shown the importance of having a hydrophilic surface for environments where the prevalence of bacteria have an affinity for hydrophobic surfaces, as is the case of periodontal pathogens, which exhibit hydrophobic activity and, therefore, are less adherent to hydrophilic surfaces [42]. We can also include A. actinomycetemcomitans and F. nucleatum which both also exhibit low adhesion to hydrophilic surfaces [43]. Therefore, in addition to the presence of silver, the bacteria–surface interaction can also be reduced by high wettability and can inhibit biofilm formation [44].

The in vitro analysis allowed us to evaluate that the different alloys do not present cellular cytotoxicity since they did not reduce the mitochondrial capacity in reducing the MTT salt measured by absorbance. In addition, it can be noted that the increase in Integrins, important cell surface receptors for the extracellular matrix, is a positive signal for cell adhesion since these receptors can alter cell behavior through the recruitment and activation of proteins such as kinases as focal adhesion kinase (FAK) and Src, resulting

in the modulation of cellular cytoskeletal rearrangement through the activation of Cofilin phosphorylation [45–47]. FAK is activated by Integrins through the disruption of an intramolecular self-inhibitory interaction between its kinase domain and the amino-terminal FERM domain [47,48]. This set of signals acts to promote cell motility, cell cycle progress, and survival in stress states triggered by extracellular signals. In our study, these extracellular signals are specific to the sites released in the culture medium that modulate this signaling cascade [41,48,49].

Cell interactions with the extracellular matrix play a key role in the cell adhesion process. For the material surface to be biocompatible, it needs to show good cell interaction. The increase in cell proliferation leads to an increase in the synthesis of the extracellular matrix and consequently increases the cell interactions. In this sense, the key role played by FAK and Integrins can be modulated by the activity of metalloproteinases that act by remodeling the collagen fibers of the extracellular matrix [47,50]. These processes allow the cell to migrate and, in tumor processes, may favor mechanisms of progression and metastasis. Matrix metalloproteinases (MMPs) act by cleaving matrisomes into bioactive extracellular matrix (ECM) molecules, promoting ECM remodeling. In bone tissue, this process may mediate cell adhesion and mechanotransduction mechanisms regulated by the regulatory activity of osteocytes that translate mechanical signals into biochemical signals [47,50]. More than half of MMP members are expressed by bone and cartilaginous cells under physiological or pathological conditions. In our results, we observed that MMP9 activity was increased in treatments with different media conditioned by biomaterial alloys. MMP9 is a marker of inflammation, tissue remodeling, wound healing, and mobilization of tissue-bound growth factors and cytokines [47,51–53]. Our data show that there was a feedback between the expression of adhesion genes and the activity of MMPs, suggesting that the coupling of these processes may be occurring in the groups that received a conditioned medium. This coupling is due to the increase in MMP9, specifically, and to the increases in FAK, Src, and Cofilin.

The presence of pathogenic microorganisms and the development of biofilms around the implant are the main factors that trigger responses by the body, such as infections and inflammation of the tissue in recovery [53]. The formation of biofilms occurs when the biological environment offers favorable conditions for bacteria to multiply in the envelope of the implanted material. In particular, the bacterial strains that surround the implant have high resistance to antibiotics, as in the case of gram-positive *Staphylococcus aureus* and *Staphylococcus epidermidis* [54,55]. For this reason, we sought to analyze the bacterial growth on the surface of the Ti7.5Mo alloy with alkaline treatment and immobilized silver using strains of *Staphylococcus aureus* and *Staphylococcus epidermidis*, as these types of bacteria have a higher incidence when related to infections associated with implantable medical devices.

The histogram shows the comparison between the two types of bacteria and the adhesive behavior of both as evaluated on the control group (G1), with alkaline treatment (G2), and with silver immobilization (G3); scanning electron microscopy images confirm what was found (Figure 7). Statistically, the values of CFU (Colony Forming Units) for the *Staphylococcus aureus* type of bacteria did not present significant differences when comparing G1 with G2; however, a smaller formation of colonies was observed for G3. Thus, the silver film played a significant role in reducing the formation of biofilms by bacteria. In relation to *Staphylococcus epidermidis*, samples G2 and G3 showed a lower colony formation when compared with *S. aureus*.

The mechanism by which silver ions interact with bacteria through the cell membrane, inhibiting various cell functions and causing cell death, has been described by several authors [56–58]. They proposed that silver ions interact with bacterial proteins and enzymes, resulting in cell membrane damage. Furthermore, they proposed that silver ions disrupt bacterial cell walls, thereby penetrating the cell membrane, binding to bacterial DNA, and inhibiting bacterial replication [34,59,60]. Another mechanism of silver's antibacterial action is through direct contact with immobilized silver nanoparticles or contact with silver nanoparticles released from a colloidal solution. In these studies, the best results were

obtained by direct contact with immobilized silver nanoparticles, far beyond substrates that released silver only in its ionic form [61,62]. According to Li et al. [63], when bacterial death occurs by direct contact with silver, the potential for lethality is even greater.

5. Conclusions

In this study, the surface of the Ti7.5Mo alloy was modified through alkaline treatment and silver immobilization to achieve a bioactive and bactericidal surface. This modification aimed to enhance cell adhesion and inhibit biofilm formation, resulting in an improved response. After the alkaline treatment, a nanoporous and homogeneous layer of sodium titanate was observed. In the samples immobilized with silver nitrate, the reproduction of the porous surface was formed by sodium titanate likely because the silver was absorbed by the porous layer. This nanoporous film alters the roughness and wettability of the surface, transforming it into an ideal surface for cell adhesion and proliferation. The alloys showed no cytotoxicity to the cells treated with the conditioned media. Furthermore, the increased expression of FAK, Src, and Cofilin demonstrated that they promote cell adhesion and ECM remodeling. In addition, the silver film played a significant role in reducing biofilm formation by both of the studied bacteria, demonstrating its biological and bactericidal properties.

In summary, the alkaline treatment on the surface of the Ti7.5Mo alloy made the surface bioactive, and the coating with silver nitrate confirmed the bactericidal effect of silver, making it feasible to carry out this surface treatment on the Ti7.5Mo alloy for biomedical applications.

Author Contributions: Conceptualization, B.L.M.d.S. and A.P.R.A.; Methodology, B.L.M.d.S., A.L.d.A.E., C.J.d.C.F., G.S.d.A., W.F.Z., P.C. and D.S.; Software, A.L.d.A.E. and A.P.R.A.; Formal analysis, B.L.M.d.S., A.L.d.A.E. and A.P.R.A.; Resources, A.L.d.A.E., C.J.d.C.F. and A.P.R.A.; Data curation, B.L.M.d.S., A.L.d.A.E., C.J.d.C.F., G.S.d.A., P.C., D.S. and A.P.R.A.; Writing—original draft, A.L.d.A.E. and A.P.R.A.; Writing—review & editing, B.L.M.d.S., A.L.d.A.E., C.J.d.C.F., G.S.d.A., P.C. and D.S.; Visualization, A.L.d.A.E. and A.P.R.A.; Supervision, A.P.R.A.; Funding acquisition, A.P.R.A. All authors have read and agreed to the published version of the manuscript.

Funding: This research was funded by the Coordenação de Aperfeiçoamento de Pessoal de Nível Superior—Brazil (CAPES)—Finance Code 001.

Institutional Review Board Statement: Not applicable.

Informed Consent Statement: Not applicable.

Data Availability Statement: The data presented in this study are available on request from the corresponding author.

Conflicts of Interest: The authors declare no conflict of interest.

References

1. Niinomi, M.; Liu, Y.; Nakai, M.; Liu, H.; Li, H. Biomedical titanium alloys with young's moduli close to that of cortical bone. *Regen. Biomater.* **2016**, *3*, 173–185. [CrossRef] [PubMed]
2. Callegari, B.; Oliveira, J.; Aristizabal, K.; Coelho, R.; Brito, P.; Wu, L.; Schell, N.; Soldera, F.; Mücklich, F.; Pinto, H. In-situ synchrotron radiation study of the aging response of Ti-6Al-4V alloy with different starting microstructures. *Mater. Charact.* **2020**, *165*, 110400. [CrossRef]
3. Callegari, B.; Oliveira, J.P.; Coelho, R.S.; Brito, P.P.; Schell, N.; Soldera, F.A.; Mücklich, F.; Sadik, M.I.; García, J.L.; Pinto, H.C. New insights into the microstructural evolution of Ti-5Al-5Mo-5V-3Cr alloy during hot working. *Mater. Charact.* **2020**, *162*, 110180. [CrossRef]
4. Long, M.; Rack, H.J. Titanium alloys in total joint replacement—A materials science perspective. *Biomaterials* **1998**, *19*, 1621–1639. [CrossRef] [PubMed]
5. Lin, C.J.H.; Ju, C.P.; Ho, W.F. Biocompatible Low Modulus Titanium Alloy for Medical Implant. U.S. Patent No. 6409852, 25 June 2002.
6. Dong, J.; Wang, W.; Zhou WZhang, S.; Li, M.; Pan, G.; Zhang, X.; Bai, J.; Zhu, C. Immunomodulatory biomaterials for implant-associated infections: From conventional to advanced therapeutic strategies. *Biomater. Res.* **2022**, *26*, 2–33. [CrossRef] [PubMed]

7. Neufeld, M.E.; Lanting, B.A.; Shehata, M.; Howard, J.L.; MacDonald, S.J.; Teeter, M.G.; Vasarhelyi, E.M. Prevalence and outcomes of unexpected positive intraoperative cultures in presumed aseptic revision hip arthroplasty. *J. Bone Jt. Surg. Am.* **2021**, *103*, 1392–1401. [CrossRef] [PubMed]
8. Xin, C.; Zhu, H.; Gao, W.; Xu, G.; Xiao, W.; Xu, Y.L. A high bioactive alkali-treated titanium surface induced by induction heat treatment. *Surf. Coat. Technol.* **2020**, *385*, 125362.
9. Ueno, T.; Tsukimura, N.; Yamada, M.; Ogawa, T. Enhanced bone-integration capability of alkali- and heat-treated nanopolymorphic titanium in micro-to-nanoscale hierarchy. *Biomaterials* **2011**, *32*, 7297–7308. [CrossRef]
10. Kawanabe, K.; Ise, K.; Goto, K.; Akiyama, H.; Nakamura, T.; Kaneuji, A.; Sugimori, T.; Matsumoto, T. A new cementless total hip arthroplasty with bioactive titanium porous-coating by alkaline and heat treatment: Average 4.8-year results. *J. Biomed. Mater. Res. B Appl. Biomater.* **2009**, *90*, 476–481. [CrossRef]
11. Escada, A.L.A.; Trujillo, N.; Ketul, C.P.; Alves Claro, A.P.R. Human dermal fibroblast adhesion on Ti-7.5Mo after TiO_2 nanotubes growth. *Mater. Sci. Forum* **2017**, *899*, 195–200. [CrossRef]
12. Claro, A.P.R.A.; Konatu, R.T.; Escada, A.L.A.; Nunes, M.C.S.; Morelli, C.V.M.; Dias-Netipanyj, M.F.; Popat, K.C.; Mantovani, D. Incorporation of silver nanoparticles on Ti7.5Mo alloy surface containing TiO_2 nanotubes arrays for promoting antibacterial coating—In Vitro and In Vivo Study. *Appl. Surf. Sci.* **2018**, *455*, 780–788. [CrossRef]
13. Kulkarni, M.; Mazare, A.; Schmuki, P.; Iglič, A.; Seifalian, A. Biomaterial surface modification of titanium and titanium alloys for medical applications. *Nanomedicine* **2014**, *111*, 615.
14. Youn, Y.H.; Lee, S.J.; Choi, G.R.; Lee, H.R.; Lee, D.; Heo, D.N.; Kim, B.S.; Bang, J.B.; Hwang, Y.S.; Correlo, V.M.; et al. Simple and facile preparation of recombinant human bone morphogenetic protein-2 immobilized titanium implant via initiated chemical vapor deposition technique to promote osteogenesis for bone tissue engineering application. *Mater. Sci. Eng. C Mater. Biol.* **2019**, *100*, 949–958. [CrossRef]
15. Khana, S.; Utsav Patel, R.; Marathey, P.; Chaudan, R.; Vora, J.; Banerjee, R.; Ray, A.; Mukhopadhyay, I. Growth of titanium dioxide nanorod over shape memory material using chemical vapor deposition for energy conversion application. *Mater. Today Proc.* **2020**, *28*, 475–479. [CrossRef]
16. Çomakl, O.; Yazıcı, M.; Kovacı, H.; Yetim, T.; Yetim, A.; Çelik, A. Tribological and electrochemical properties of TiO_2 films produced on Cp-Ti by sol-gel and SILAR in bio-simulated environment. *Surf. Coat. Technol.* **2018**, *352*, 513–521. [CrossRef]
17. Svagrova, K.; Horkavcova, D.; Jablonska, E.; Helebrant, A. Titania-based sol–gel coatings with Ag, Ca-P applied on titanium substrate developed for implantation. *J. Biomed. Mater. Res. B Appl. Biomater.* **2022**, *110*, 115–124. [CrossRef] [PubMed]
18. Zinjarde, S.S. Bio-inspired nanomaterials and their applications as antimicrobial agents. *Chron. Young Sci.* **2012**, *3*, 74. [CrossRef]
19. Siddiqi, S.K.; Husen, A.; Rao, R.A.K. A review on biosynthesis of silver nanoparticles and their biocidal properties. *J. Nanobiotechnol.* **2018**, *16*, 2–28. [CrossRef]
20. Dhas, T.S.; Ganesh, V.; Kumar, V. Facile synthesis of silver chloride nanoparticles using marine alga and its antibacterial efficacy. *Spectrochim. Acta Mol. Biomol. Spectrosc.* **2014**, *120*, 416–420. [CrossRef]
21. Escada, A.L.A.; Machado, J.P.B.; Schneider, S.G.; Alves Rezende, M.C.R.; Alves Claro, A.P.R. Biomimetic calcium phosphate coating on Ti-7.5Mo alloy for dental application. *J. Mater. Sci. Mater. Med.* **2011**, *22*, 2457–2465. [CrossRef]
22. Escada, A.L.A.; Machado, J.P.B.; Rodrigues, D., Jr.; Alves Claro, A.P.R. Surface characterization of Ti7.5Mo alloy modified by biomimetic method. *Surf. Coat. Technol.* **2010**, *205*, 383–387. [CrossRef]
23. Escada, A.L.A.; Camargo, S.E.A.; Vasconcellos, L.M.R.; Milhan, N.V.M.; Alves Claro, A.P.R. Cytotoxicity analysis of Ti-7.5Mo alloy after biomimetic surface treatment to use as dental materials. *Mater. Res.-Ibero-Am. J. Mater.* **2017**, *20*, 4–8. [CrossRef]
24. Kim, H.S.; Kumbar, S.G. Biomaterial-directed cell behavior for tissue engineering. *Curr. Opin. Biomed. Eng.* **2021**, *17*, 100260. [CrossRef] [PubMed]
25. Ferraris, S.; Spriano, S. Antibacterial Titanium Surfaces for Medical Implants. *Mater. Sci. Eng. C.* **2016**, *61*, 965–978. [CrossRef] [PubMed]
26. Besinis, A.; Hadi, S.D.; Le, H.; Tredwin, C.; Handy, R. Antibacterial activity and biofilm inhibition by surface modified titanium alloy medical implants following application of silver, titanium dioxide and hydroxyapatite nanocoatings. *Nanotoxicology* **2017**, *11*, 327–338. [CrossRef] [PubMed]
27. Boyan, B.D.; Cheng, A.; Olivares-Navarrete, R.; Schwartz, Z. Implant surface design regulates mesenchymal stem cell differentiation and maturation. *Adv. Dent. Res.* **2016**, *28*, 10–17. [CrossRef] [PubMed]
28. Bressan, E.; Sbricoli, L.; Guazzo, R.; Tocco, I.; Roman, M.; Vindigni, V.; Stellini, E.; Gardin, C.; Ferroni, L.; Sivolella, S.; et al. Nanostructured surfaces of dental implants. *Int. J. Mol. Sci.* **2013**, *14*, 1918–1931. [CrossRef] [PubMed]
29. Wu, B.; Tang, Y.; Wang, K.; Zhou, X.; Xiang, L. Nanostructured Titanium Implant Surface Facilitating Osseointegration from Protein Adsorption to Osteogenesis: The Example of TiO2NTAs. *Int. J. Nanomed.* **2022**, *17*, 1865–1879. [CrossRef]
30. Ogura, N.; Berger, M.B.; Srivas, P.; Hwang, S.; Li, J.; Cohen, D.J.; Schwarts, Z.; Boyan, B.D.; Dandhage, K.H. Tailoring of TiAl6V4 Surface Nanostructure for Enhanced In Vitro Osteoblast Response via Gas/Solid (Non-Line-of-Sight) Oxidation / Reduction Reactions. *Biomimetics* **2022**, *7*, 117. [CrossRef]
31. Medvedev, A.E.; Ng, H.P.; Lapovok, R.; Estrin, Y.; Lowe, T.C. Effect of bulk microstructure of commercially pure titanium on surface characteristics and fatigue properties after surface modification by sand blasting and acid-etching. *J. Behav. Biomed. Mater.* **2016**, *57*, 55–68. [CrossRef]

32. Kataoka, Y.; Tamaki, Y.; Miyazaki, T. Synergistic responses of superficial chemistry and micro topography of titanium created by wire-type electric discharge machining. *Bio-Med. Mater. Eng.* **2011**, *21*, 113–121. [CrossRef]
33. Eom, T.G.; Jeon, G.R.; Jeong, C.M. Estudo experimental da resposta óssea a implantes com revestimento de hidroxiapatita: Contato osso-implante e teste de torque de remoção. *Cir. Oral Med. Oral Patol. Oral E Radiol. Oral* **2012**, *114*, 411–418. [CrossRef]
34. Mocanu, A.; Furtos, G.; Rapuntean, S.; Horovitz, O.; Flore, C.; Garbo, C.; TomoaiaCotisel, M. Synthesis, characterization and antimicrobial effects of composites based on multi-substituted hydroxyapatite and silver nanoparticles. *Appl. Surf. Sci.* **2014**, *298*, 225–235. [CrossRef]
35. Ranj, N.; Salaieac, A.B.; Huirong, L.; Christopher, T.; Richard, D.H. The biocompatibility of silver and nanohydroxyapatite coatings on titanium dental implants with human primary osteoblast cells. *Mater. Sci. Eng. C* **2020**, *17*, 100260.
36. Barthes, J.; Cazzola, M.; Muller, C. Controlling porous titanium/soft tissue interactions with an innovative surface chemical treatment: Responses of macrophages and fibroblasts. *Mater. Sci. Eng. C* **2020**, *112*, 110845. [CrossRef]
37. Vilardell, A.M.; Cinca, N.; Garcia-Girald, N. In-vitro study of hierarchical structures: Anodic oxidation and alkaline treatments onto highly rough titanium cold gas spray coatings for biomedical applications. *Mater. Sci. Eng. C* **2018**, *91*, 589–596. [CrossRef]
38. Fan, H.; Guo, Z. Bioinspired surfaces with wettability: Biomolecule adhesion behaviors. *Biomater. Sci.* **2020**, *8*, 1502–1535. [CrossRef]
39. Polini, A.; Yang, F. Physicochemical characterization of nanofiber composites. In *Nanofiber Composites for Biomedical Applications*; Woodhead Publishing: Cambridge, UK, 2017; pp. 97–115.
40. Polo-Corrales, L.; Latorre-Esteves, M.; Ramirez-Vick, J.E. Scaffold design for bone regeneration. *J. Nanosci. Nanotechnol.* **2014**, *14*, 15–56. [CrossRef]
41. Achinas, S.; Charalampogiannis, N.; Euverink, G.J. A brief recap of microbial adhesion and biofilms. *Appl. Sci.* **2019**, *9*, 2801. [CrossRef]
42. Zhang, X.W.L.; Levänena, E. Superhydrophobic surfaces for the reduction of bacterial adhesion. *RSC Adv.* **2013**, *3*, 12003–12020. [CrossRef]
43. Almaguer-Flores, A.; Olivares-Navarrete, R.; Wieland, M.; Ximenez-Fyvie, L.A.; Schwartz, Z.; Boyan, B.D. Influence of topography and hydrophilicity on initial oral biofilm formation on microstructured titanium surfaces in vitro. *Clin. Oral Implant. Res.* **2012**, *23*, 301–307. [CrossRef]
44. Mi, L.; Jiang, S. Integrated antimicrobial and nonfouling zwitterionic polymers. *Angew. Chem. Int. Ed. Engl.* **2014**, *53*, 1746–1754. [CrossRef]
45. Manicourt, D.H.; Lefebvre, V. An assay for matrix metalloproteinases and other proteases acting on proteoglycans, casein, or gelatin. *Anal. Biochem.* **1993**, *9*, 171–215. [CrossRef]
46. Daley, W.P.; Peters, S.B.; Larsen, M. Extracellular matrix dynamics in development and regenerative medicine. *J. Cell Sci.* **2008**, *121*, 255–264. [CrossRef]
47. Aiyelabegan, H.T.; Sadroddiny, E. Fundamentals of protein and cell interactions in biomaterials. *Biomed. Pharmacother.* **2018**, *8*, 956–970. [CrossRef]
48. da Costa Fernandes, C.J.; Ferreira, M.R.; Bezerra, F.J.B.; Zambuzzi, W.F. Zirconia stimulates ECM-remodeling as a prerequisite to pre-osteoblast adhesion/proliferation by possible interference with cellular anchorage. *J. Mater. Sci. Mater. Med.* **2018**, *29*, 41. [CrossRef]
49. Da Silva, R.A.; da Silva Feltran, G.; Ferreira, M.R.; Wood, P.F.; Bezerra, F.; Zambuzzi, W.F. The Impact of Bioactive Surfaces in the Early Stages of Osseointegration: An in Vitro comparative study evaluating the HAnano® and SLActive® Super Hydrophilic Surfaces. *Biomed. Res. Int.* **2020**, *2020*, 3026893. [CrossRef]
50. Tokuhara, C.K.; Santesso, M.R.; de Oliveira, G.S.N.; da Ventura, T.M.S.; Doyama, J.T.; Zambuzzi, W.F.; de Oliveira, R.C. Updating the role of matrix metalloproteinases in mineralized tissue and related diseases. *J. Appl. Oral Sci.* **2019**, *27*, 1–14. [CrossRef]
51. Machado, M.I.P.; Gomes, A.M.; Rodrigues, M.F.; Silva Pinto, T.; da Costa Fernandes, C.J.; Bezerra, F.J.; Zambuzzi, W.F. Cobalt-chromium-enriched medium ameliorates shear-stressed endothelial cell performance. *J. Trace Elem. Med. Biol.* **2019**, *54*, 163–171. [CrossRef]
52. Zambuzzi, W.F.; Paiva, K.B.S.; Menezes, R.; Oliveira, R.C.; Taga, R.; Granjeiro, J.M. MMP-9 and CD68(+) cells are required for tissue remodeling in response to natural hydroxyapatite. *J. Mol. Histol.* **2009**, *40*, 301–309. [CrossRef]
53. Rooprai, H.K.; Martin, A.J.; King, A.; Appadu, U.D.; Jones, H.; Selway, R.P.; Gullan, R.W.; Pilkington, G.J. Comparative gene expression profiling of ADAMs, MMPs, TIMPs, EMMPRIN, EGF-R and VEGFA in low grade meningioma. *Int. J. Oncol.* **2016**, *49*, 2309–2318. [CrossRef]
54. de Breij, A.; Riool, M.; Kwakman, P.H.S.; de Boer, L.; Cordfunke, R.A.; Drijfhout, J.W.; Cohen, O.; Emanuel, N.; Zaat, S.A.J.; Nibbering, H.; et al. Prevention of Staphylococcus aureus biomaterial-associated infections using a polymer-lipid coating containing the antimicrobial peptide OP-145. *J. Control. Release* **2016**, *222*, 1–8. [CrossRef]
55. Nune, K.C.; Somani, M.C.; Spencer, C.T.; Misra, R.D.K. Cellular response of Staphylococcus aureus to nanostructured metallic biomedical devices: Surface binding and mechanism of disruption of colonization. *Mater. Technol.* **2017**, *32*, 22–31. [CrossRef]
56. Li, D.; Liu, S.; Ma, Y.; Liu, S.; Liu, Y.; Ding, J. Biomaterials That Induce Immunogenic Cell Death. *Small Methods* **2023**, *7*, 2300204. [CrossRef]
57. Gla, H.; Jonitz-Heincke, A.; Petters, J.; Lukas, J.; Bader, R.; Hermann, A. Corrosion Products from Metallic Implants Induce ROS and Cell Death in Human Motoneurons In Vitro. *J. Funct. Biomater.* **2023**, *14*, 392.

58. Zhang, Y.; Doan, B.-T.; Gasser, G. Metal-Based Photosensitizers as Inducers of Regulated Cell Death Mechanisms. *Chem. Rev.* **2023**, *123*, 10135–10155. [CrossRef]
59. Prabhu, S.; Poulose, E.K. Silver Nanoparticles: Mechanism of antimicrobial action, synthesis, medical applications, and toxicity effects. *Int. Nano Lett.* **2012**, *2*, 1–10. [CrossRef]
60. Iqbal, N.; Kadir, M.R.A.; Mahmood, N.H.B.; Iqbal, S.; Almasi, D.; Naghizadeh, F.; Kamarul, T. Characterization and biological evaluation of silver containing fluoroapatite nanoparticles prepared through microwave synthesis. *Ceram. Int.* **2015**, *41*, 6470–6477. [CrossRef]
61. Lan, M.Y.; Liu, C.P.; Huang, H.H.; Lee, S.W. Both enhanced biocompatibility and antibacterial activity in Ag-decorated TiO_2 nanotubes. *PLoS ONE* **2013**, *8*, e75364. [CrossRef]
62. Agnihotri, S.; Mukherji, S.; Mukherji, S. Immobilized silver nanoparticles enhance contact killing and show highest efficacy: Elucidation of the mechanism of bactericidal action of silver. *Nanoscale* **2013**, *5*, 7328–7340. [CrossRef]
63. Li, Y.; Leung, W.K.; Yeung, K.L.; Lau, P.S.; Kwan, J.K.C. A multilevel antimicrobial coating based on polymer-encapsulated ClO_2. *Langmuir* **2009**, *25*, 13472–13480. [CrossRef] [PubMed]